Maximum Torque Per Ampere Algorithm for Five-Phase Synchronous Reluctance Machines

Andrea Cervone, *Student Member, IEEE*, and Obrad Dordevic, *Member, IEEE*

***Abstract*—This paper presents a Maximum Torque Per Ampere strategy for a five-phase synchronous reluctance drive. The approach is developed considering general machine parameters and is formalized as a constrained optimization problem. The optimal solution is found analytically by using Lagrange's multipliers method and is based on the computation of the eigenvalues and eigenvectors of the inductance derivatives matrix. The proposed approach is evaluated both numerically and experimentally. It is also compared with other current references control strategies, effectively showing a reduction of the machine RMS currents for the same developed torque. The same approach can also be extended to machines with a different number of phases.**

***Index Terms*—Multiphase machines, Synchronous Reluctance Machines, Maximum Torque Per Ampere, Losses Minimization.**

I. Introduction

SYNCHRONOUS reluctance machines (SynRMs) are a well-known technology that for long has attracted the interest of the electrical scientific community. This is because of its simple construction and because it can achieve the synchronous operation without requiring an excitation coil or permanent magnets placed on the rotor [1], [2]. The torque development in a SynRM is based on variable reluctance effects, which can be obtained by properly designing the rotor of the machine, that can be realized either with salient poles or with flux barriers [3]. The stator of a SynRM is instead of a standard cylindrical surface, and its phase windings can be designed either with a concentrated or with a distributed layout.

It is currently recognized that the employment of more than three phases (i.e., of a multiphase electrical machine) offers several benefits over standard three-phase solutions, that can be of interest especially in high-power and high-reliability applications [4]–[6]. Indeed, the input power can be conveniently split into multiple phases, which allows reduction of the rated voltage or current of the supplying converter, and the intrinsic redundancy of these configurations allows the continuous machine operation even after fault occurrence, as long as it is possible to generate a rotating magnetic field at the air-gap (although with some performance derating).

Manuscript received Month xx, 2xxx; revised Month xx, xxxx; accepted Month x, xxxx.

A. Cervone is with the Department of Electrical Engineering and Information Technology, University of Naples Federico II, 80125, Naples, Italy (e-mail: andrea.cervone@unina.it)

O. Dordevic is with the Faculty of Engineering and Technology, Liverpool John Moores University, Liverpool L3 3AF, U.K. (e-mail: O.Dordevic@ljmu.ac.uk)

As known, another relevant benefit offered by multiphase configurations is the possibility to enhance the torque development by using non-sinusoidal currents [5]. This capability has been successfully exploited for induction machines and permanent magnet synchronous machines, but it has instead been seldom addressed for SynRMs. Indeed, while there are many proposed strategies on how to improve the torque characteristics for three-phase SynRMs [7]–[14], not many studies have been conducted for multiphase ones.

In this case, the most notable results have been obtained in [15]–[17], where it has been shown that, for a five-phase SynRM with concentrated windings, a torque enhancement can be obtained by applying a proper third harmonic injection into the machine phase currents. Indeed, in this case, the injected third harmonic currents can generate a third harmonic in the spatial magnetomotive field in the air gap. This additional field can be exploited to develop an additional contribution to the electromagnetic torque other than the one produced by the fundamental currents. By using a standard analysis approach based on a Vector Space Decomposition (VSD), the injection ratio for the machine phase currents has been selected based on the mutual cross-coupling existing between the $\alpha - \beta$ and the $x - y$ planes of the transformed VSD components. This capability has then also been exploited in [18], [19] to compare different rotor designs for five-phase SynRMs, and has been shown that, while rotor designs based on flux-barriers are more suited for purely sinusoidal current excitations, for a salient poles structure it is possible to achieve a consistent torque development enhancement via the third harmonic injection, because of the higher mutual coupling effects among different VSD planes.

In the same years, the use of non-sinusoidal currents was also applied to SynRMs with a different number of phases (e.g., six-phase [20] and nine-phase [21]), using a simple strategy based on forcing a piece-wise constant current to each phase according to the physical position of its conductors with respect to the salient poles of the rotor. However, no analytical investigations were made to optimize the currents distribution, and no further analyses were made after that. More recently, multiphase SynRMs have started gaining back some interest in the technical community. However, up to this day, the most recent publications have been mainly focused on some analysis and design aspects [22]–[26], while advanced control techniques have not been investigated yet.

This paper further analyses the harmonic injection capabilities by presenting a Maximum Torque Per Ampere (MTPA) strategy for a five-phase SynRM drive (Fig. 1). The proposed algorithm is formalized as a constrained optimization problem,

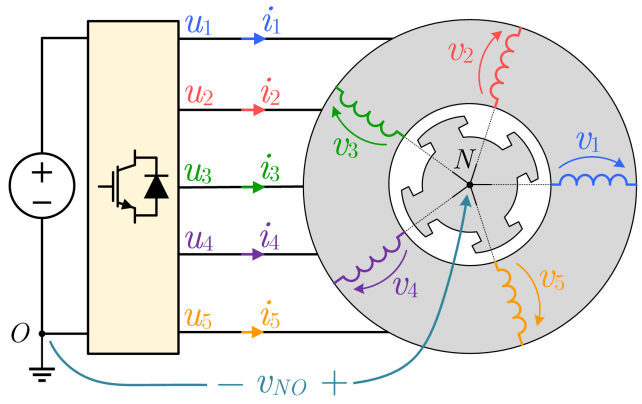

Fig. 1. Schematic representation of a five-phase synchronous reluctance machine drive.

and a general solution is provided analytically. It is shown that, depending on the machine parameters, multiple harmonics (including additional higher-order contributions) can be simultaneously exploited to develop the desired torque while optimizing the system performances. Indeed, the optimal solution generally results in a set of non-sinusoidal phase currents, and intrinsically considers all the possible harmonic interactions which can be exploited for torque development. The proposed algorithm is validated both numerically and experimentally with respect to a salient pole SynRM, and is compared both to the sole exploitation of the sinusoidal current components and to the third harmonic injection strategy developed in [15], [16]. The approach, which is developed for a generic five-phase SynRM, can be also easily extended for a machine with a different number of phases.

The paper is structured as follows. First, Section II summarizes the mathematical model of the drive. Then, Section III describes the proposed MTPA algorithm, which is particularized in Section IV with an experimental prototype. Finally, Section V summarizes the conclusions of this work.

II. Mathematical Model

A. Phase Variable Model

Under the linearity hypothesis, the flux induced in each stator winding is given by the superimposed contribution of the magnetic field produced by all the phase currents. By using matrix notation and by denoting with the subscript "ph" the phase variable reference frame, this relationship can be expressed as:

$$\boldsymbol{\lambda}_{\rm ph} = \boldsymbol{L}_{\rm ph}(\theta_{el}) \cdot \boldsymbol{i}_{\rm ph} \tag{1}$$

where $\boldsymbol{\lambda}_{\rm ph} = [\lambda_1, \dots, \lambda_5]^{\rm T}$ is the 5×1 vector of fluxes induced in the machine windings, $\boldsymbol{i}_{\rm ph} = [i_1, \dots, i_5]^{\rm T}$ is the 5×1 vector of phase currents, and

$$\boldsymbol{L}_{\rm ph}(\theta_{el}) = \begin{bmatrix} L_{1,1}(\theta_{el}) & L_{1,2}(\theta_{el}) & \cdots & L_{1,5}(\theta_{el}) \\ L_{2,1}(\theta_{el}) & L_{2,2}(\theta_{el}) & \cdots & L_{2,5}(\theta_{el}) \\ \vdots & \vdots & \ddots & \vdots \\ L_{5,1}(\theta_{el}) & L_{5,2}(\theta_{el}) & \cdots & L_{5,5}(\theta_{el}) \end{bmatrix} \tag{2}$$

is the 5×5 inductances matrix.

Due to the variable reluctance effects, all the terms in (2) are periodic functions of the electrical position $\theta_{el} = P_p\,\theta$, where P_p is number of pole pairs of the machine and θ is the mechanical angle of the rotor. Since the rotor is usually designed with an even number of salient poles, each term $L_{k,h}(\theta_{el})$ (with $h, k = 1, \dots, 5$) can be analysed in the Fourier domain as a superposition of a constant term and of multiple even order harmonics varying with θ_{el}. From the energy conservation principle, it is known that $\boldsymbol{L}_{\rm ph}(\theta_{el})$ is symmetric and positive definite. Moreover, for symmetry reasons, it also results that $L_{h+1,k+1}(\theta_{el}) = L_{h,k}(\theta_{el} - 2\pi/5)$ for all h and k.

As known, in the linearity hypothesis, the electromagnetic energy W_{em} stored in the machine and the electromagnetic coenergy $W^c_{em} = \boldsymbol{\lambda}^{\rm T}_{\rm ph} \cdot \boldsymbol{i}_{\rm ph} - W_{em}$ are equal and given by:

$$W_{em} = W^c_{em} = \frac{1}{2}\,\boldsymbol{\lambda}^{\rm T}_{\rm ph} \cdot \boldsymbol{i}_{\rm ph} = \frac{1}{2}\,\boldsymbol{i}^{\rm T}_{\rm ph} \cdot \boldsymbol{L}_{\rm ph}(\theta_{el}) \cdot \boldsymbol{i}_{\rm ph} \tag{3}$$

Then, the electromagnetic torque T_{em} developed by the machine can be computed as the partial derivative of the coenergy W^c_{em} with respect to the rotor position θ, computed at constant currents. From (3) it results:

$$T_{em} = \frac{\partial W^c_{em}}{\partial \theta} = \frac{1}{2}\,\boldsymbol{i}^{\rm T}_{\rm ph} \cdot \boldsymbol{L}'_{\rm ph}(\theta_{el}) \cdot \boldsymbol{i}_{\rm ph} \tag{4}$$

The matrix $\boldsymbol{L}'_{\rm ph}(\theta_{el}) = \partial \boldsymbol{L}_{\rm ph}/\partial\theta = P_p \cdot \partial \boldsymbol{L}_{\rm ph}/\partial\theta_{el}$ is responsible for the torque development due to variable reluctance effects. Again, it is symmetric and its coefficients are periodic in θ_{el} but, in general, it is not positive definite.

The winding terminal voltages are given by the contributions of the resistive drop and the induced back-EMFs:

$$\boldsymbol{v}_{\rm ph} = R \cdot \boldsymbol{i}_{\rm ph} + \frac{\rm d}{{\rm d}t}\left(\boldsymbol{L}_{\rm ph} \cdot \boldsymbol{i}_{\rm ph}\right) \tag{5}$$

where $\boldsymbol{v}_{\rm ph} = [v_1, \dots, v_5]^{\rm T}$ is the 5×1 vector of winding terminal voltages, and R is the winding resistance. Considering the single-star configuration of Fig. 1, by applying Kirchhoff's laws it also results that:

$$\boldsymbol{v}_{\rm ph} = \boldsymbol{u}_{\rm ph} - \boldsymbol{1}_5 \cdot v_{NO} \tag{6}$$

$$\boldsymbol{1}^{\rm T}_5 \cdot \boldsymbol{i}_{\rm ph} = \sum\nolimits_{k=1}^{5} i_k = 0 \tag{7}$$

where $\boldsymbol{u}_{\rm ph} = [u_1, \dots, u_5]^{\rm T}$ is the 5×1 vector of VSI leg voltages, $\boldsymbol{1}_5 = [1, 1, 1, 1, 1]^{\rm T}$, and v_{NO} is the voltage between the machine neutral point N and the VSI reference node O.

To sum up, by combining (4)-(7), the machine equations in the phase variable domain are:

$$\frac{\rm d}{{\rm d}t}\left(\boldsymbol{L}_{\rm ph} \cdot \boldsymbol{i}_{\rm ph}\right) + R \cdot \boldsymbol{i}_{\rm ph} = \boldsymbol{v}_{\rm ph} = \boldsymbol{u}_{\rm ph} - \boldsymbol{1}_5 \cdot v_{NO} \tag{8a}$$

$$\boldsymbol{1}^{\rm T}_5 \cdot \boldsymbol{i}_{\rm ph} = \sum\nolimits_{k=1}^{5} i_k = 0 \tag{8b}$$

$$T_{em} = \frac{1}{2}\,\boldsymbol{i}^{\rm T}_{\rm ph} \cdot \boldsymbol{L}'_{\rm ph}(\theta_{el}) \cdot \boldsymbol{i}_{\rm ph} \tag{8c}$$

B. VSD Model

The machine model can be reformulated by applying to each 5×1 vector $\boldsymbol{z}_{\rm ph} = [z_1, \dots, z_5]^{\rm T}$ the variable transformation known as Vector Space Decomposition (VSD) [27], [28]:

$$\boldsymbol{z}_{\rm VSD} = \boldsymbol{C} \cdot \boldsymbol{z}_{\rm ph} \quad \Leftrightarrow \quad \boldsymbol{z}_{\rm ph} = \boldsymbol{C}^{-1} \cdot \boldsymbol{z}_{\rm VSD} \tag{9}$$

where $\boldsymbol{z}_{\rm VSD} = [z_\alpha, z_\beta, z_x, z_y, z_0]^{\rm T}$ is the 5×1 transformed set, and $\boldsymbol{C}$ is the generalized Clarke's transformation matrix:

$$\boldsymbol{C} = \sqrt{\frac{2}{5}} \begin{bmatrix} \cos(0\cdot\gamma) & \cos(1\cdot\gamma) & \cdots & \cos(4\cdot\gamma) \\ \sin(0\cdot\gamma) & \sin(1\cdot\gamma) & \cdots & \sin(4\cdot\gamma) \\ \cos(0\cdot3\cdot\gamma) & \cos(1\cdot3\cdot\gamma) & \cdots & \cos(4\cdot3\cdot\gamma) \\ \sin(0\cdot3\cdot\gamma) & \sin(1\cdot3\cdot\gamma) & \cdots & \sin(4\cdot3\cdot\gamma) \\ 1/\sqrt{2} & 1/\sqrt{2} & \ldots & 1/\sqrt{2} \end{bmatrix} \quad (10)$$

with $\gamma = 2\pi/5$ denoting the angular shift between two consecutive axes of the machine. It can be verified that the matrix defined as per (10) is unitary, meaning that $\boldsymbol{C}^{\rm T} = \boldsymbol{C}^{-1}$.

By applying (9) to the model (8), it results that:

$$\frac{\rm d}{{\rm d}t}\left(\boldsymbol{C}\cdot\boldsymbol{L}_{\rm ph}(\theta_{el})\cdot\boldsymbol{C}^{\rm T}\cdot\boldsymbol{i}_{\rm VSD}\right) + R\cdot\boldsymbol{i}_{\rm VSD} = \\ = \boldsymbol{v}_{\rm VSD} = \boldsymbol{u}_{\rm VSD} - \boldsymbol{C}\cdot\boldsymbol{1}_5\cdot v_{NO} \quad (11a)$$

$$\boldsymbol{1}_5^{\rm T}\cdot\boldsymbol{C}^{\rm T}\cdot\boldsymbol{i}_{\rm VSD} = 0 \quad (11b)$$

$$T_{em} = \frac{1}{2}\,\boldsymbol{i}_{\rm VSD}^{\rm T}\cdot\boldsymbol{C}\cdot\boldsymbol{L}'_{\rm ph}(\theta_{el})\cdot\boldsymbol{C}^{\rm T}\cdot\boldsymbol{i}_{\rm VSD} = \\ = \frac{1}{2}\,\boldsymbol{i}_{\rm VSD}^{\rm T}\cdot\frac{\partial\left(\boldsymbol{C}\cdot\boldsymbol{L}_{\rm ph}(\theta_{el})\cdot\boldsymbol{C}^{\rm T}\right)}{\partial\theta}\cdot\boldsymbol{i}_{\rm VSD} \quad (11c)$$

From the Clarke's matrix in (10) it results that $\boldsymbol{C}\cdot\boldsymbol{1}_5 = [0,0,0,0,\sqrt{5}]^{\rm T}$. Therefore, the equation (11b) simply means that $i_0 = 0$, while equation (11a) means that the dynamics of the $\alpha-\beta$ and $x-y$ components are not influenced by v_{NO}. As a result, the zero-sequence components of the system can be discarded from the drive mathematical model (11), which can be therefore reformulated as:

$$\frac{\rm d}{{\rm d}t}\left(\boldsymbol{L}_{\rm eq}(\theta_{el})\cdot\boldsymbol{i}_{\rm eq}\right) + R\cdot\boldsymbol{i}_{\rm eq} = \boldsymbol{v}_{\rm eq} = \boldsymbol{u}_{\rm eq} \quad (12a)$$

$$T_{em} = \frac{1}{2}\,\boldsymbol{i}_{\rm eq}^{\rm T}\cdot\boldsymbol{L}'_{\rm eq}(\theta_{el})\cdot\boldsymbol{i}_{\rm eq} \quad (12b)$$

where $\boldsymbol{z}_{\rm eq} = [z_\alpha, z_\beta, z_x, z_y]^{\rm T}$ is the 4×1 equivalent set related to each variable $\boldsymbol{z}$, while:

$$\boldsymbol{L}_{\rm eq}(\theta_{el}) = \begin{bmatrix} L_{\alpha\alpha}(\theta_{el}) & L_{\alpha\beta}(\theta_{el}) & L_{\alpha x}(\theta_{el}) & L_{\alpha y}(\theta_{el}) \\ L_{\beta\alpha}(\theta_{el}) & L_{\beta\beta}(\theta_{el}) & L_{\beta x}(\theta_{el}) & L_{\beta y}(\theta_{el}) \\ L_{x\alpha}(\theta_{el}) & L_{x\beta}(\theta_{el}) & L_{xx}(\theta_{el}) & L_{xy}(\theta_{el}) \\ L_{y\alpha}(\theta_{el}) & L_{y\beta}(\theta_{el}) & L_{yx}(\theta_{el}) & L_{yy}(\theta_{el}) \end{bmatrix} \quad (13)$$

is the equivalent inductances matrix concerning the mutual interaction between the transformed currents. Considering (13), the matrix $\boldsymbol{L}_{\rm eq}(\theta_{el})$ is obtained by only considering the first 4 rows and 4 columns of the 5×5 matrix $(\boldsymbol{C}\cdot\boldsymbol{L}_{\rm ph}(\theta_{el})\cdot\boldsymbol{C}^{\rm T})$ (which instead also considered the effect of the zero-sequence components). This matrix, similarly to $\boldsymbol{L}_{\rm ph}$, is also a symmetric and positive-definite matrix, and its coefficients are periodic functions of the rotor electrical position θ_{el}. The matrix $\boldsymbol{L}'_{\rm eq}(\theta_{el})$, appearing in the second equation of (12), is simply given as $\boldsymbol{L}'_{\rm eq}(\theta_{el}) = \partial\boldsymbol{L}_{\rm eq}/\partial\theta = P_p\cdot\partial\boldsymbol{L}_{\rm eq}/\partial\theta_{el}$.

III. MTPA Strategy

The machine control is typically aimed at developing a desired electromagnetic torque T^*_{em} coming, for example, from a speed controller. This can be done by properly acting on the machine phase currents and, therefore, by properly computing a reference current set to be tracked. The computation of the current references required to develop the desired torque can be addressed either in the phase variable domain, by referring to the model analysed in Section II.A, or in the transformed (VSD) domain, by referring to the model analysed in Section II.B. The results of the two approaches are equivalent and are simply linked by the transformation (9). Here, this problem will be analysed in the transformed domain, since the constraint on the sum of the phase currents (7) is intrinsically included in the model (12).

A. MTPA Problem Formulation

Considering (12b), the torque development requirement can be formalized as an algebraic constraint on the reference current set $\boldsymbol{i}^*_{\rm eq} = [i^*_\alpha, i^*_\beta, i^*_x, i^*_y]^{\rm T}$ to be computed. As a result, there are 3 degrees of freedom, which can be exploited to maximize the system performances. A convenient and commonly adopted choice is to minimize the equivalent current [13]:

$$I_m = ||\boldsymbol{i}_{\rm ph}|| = \sqrt{\boldsymbol{i}_{\rm ph}^{\rm T}\cdot\boldsymbol{i}_{\rm ph}} = \sqrt{\sum\nolimits_{k=1}^{5} i_k^2} \quad (14)$$

The minimization of I_m for a given reference torque is equivalent to the maximization of the torque for a given I_m, meaning that this approach can be interpreted as a Maximum Torque Per Ampere (MTPA) strategy. As known, the minimization of I_m also leads to a reduction of the overall machine stator losses $p_{Cu} = R\cdot\sum_{k=1}^{5} i_k^2 = R\cdot I_m^2$, which often represent the main contribution to the overall losses [13].

Considering the VSD transformation (9) with the chosen unitary Clarke transformation matrix (10), and since $i_0 = 0$ (because of the single-isolated neutral point configuration) the current I_m in (14) can be reformulated as:

$$I_m = \sqrt{\boldsymbol{i}_{\rm ph}^{\rm T}\cdot\boldsymbol{i}_{\rm ph}} = \sqrt{\boldsymbol{i}_{\rm VSD}^{\rm T}\cdot\boldsymbol{C}\cdot\boldsymbol{C}^{\rm T}\cdot\boldsymbol{i}_{\rm VSD}} = \\ = \sqrt{\boldsymbol{i}_{\rm VSD}^{\rm T}\cdot\boldsymbol{i}_{\rm VSD}} = \sqrt{i_\alpha^2 + i_\beta^2 + i_x^2 + i_y^2 + i_0^2} = \\ = \sqrt{i_\alpha^2 + i_\beta^2 + i_x^2 + i_y^2} = \sqrt{\boldsymbol{i}_{\rm eq}^{\rm T}\cdot\boldsymbol{i}_{\rm eq}} \quad (15)$$

Therefore, the considered MTPA strategy can be formulated as the constrained optimization problem:

$$\min_{\boldsymbol{i}_{\rm eq}}\{\boldsymbol{i}_{\rm eq}^{\rm T}\cdot\boldsymbol{i}_{\rm eq}\} \quad \text{subject to} \quad \boldsymbol{i}_{\rm eq}^{\rm T}\cdot(\boldsymbol{L}'_{\rm eq}/2)\cdot\boldsymbol{i}_{\rm eq} = T^*_{em} \quad (16)$$

where the periodic dependence of $\boldsymbol{L}'_{\rm eq}$ on θ_{el} has been omitted for notation compactness.

B. MTPA Problem Solution

A useful tool to solve constrained optimization problems is Lagrange's multipliers method. This approach has also been used for different kinds of machines in [13], [14] and it is here particularized for the considered five-phase SynRM. The Lagrangian function for (16) can be chosen as:

$$\mathcal{L}(\boldsymbol{i}_{\rm eq}, \mu) = \boldsymbol{i}_{\rm eq}^{\rm T}\cdot\boldsymbol{i}_{\rm eq} - \mu\cdot\left(\boldsymbol{i}_{\rm eq}^{\rm T}\cdot(\boldsymbol{L}'_{\rm eq}/2)\cdot\boldsymbol{i}_{\rm eq} - T^*_{em}\right) \quad (17)$$

where μ is the Lagrange multiplier related to the torque development requirement. The optimal solution of (16) nullifies the gradient of (17), and can be found by solving the system

$$\partial\mathcal{L}/\partial\boldsymbol{i}_{\rm eq} = 2\,\boldsymbol{i}_{\rm eq} - \mu\cdot(\boldsymbol{L}'_{\rm eq}/2)\cdot\boldsymbol{i}_{\rm eq} = \boldsymbol{0} \quad (18a)$$

$$\partial\mathcal{L}/\partial\mu = \boldsymbol{i}_{\rm eq}^{\rm T}\cdot(\boldsymbol{L}'_{\rm eq}/2)\cdot\boldsymbol{i}_{\rm eq} - T^*_{em} = 0 \quad (18b)$$

The vector equation of (18a) can be rewritten as:

$$\boldsymbol{L}'_{\mathrm{eq}} \cdot \boldsymbol{i}_{\mathrm{eq}} = (4/\mu) \cdot \boldsymbol{i}_{\mathrm{eq}} = \nu \cdot \boldsymbol{i}_{\mathrm{eq}} \tag{19}$$

This means that, if the vector $\boldsymbol{i}^*_{\mathrm{eq}}$ is the optimal solution of (16), then the vector $\boldsymbol{L}'_{\mathrm{eq}} \cdot \boldsymbol{i}^*_{\mathrm{eq}}$ is parallel to $\boldsymbol{i}^*_{\mathrm{eq}}$ itself. In other words, $\boldsymbol{i}^*_{\mathrm{eq}}$ is an eigenvector of $\boldsymbol{L}'_{\mathrm{eq}}$, and $\nu = 4/\mu$ is the corresponding eigenvalue.

Since $\boldsymbol{L}'_{\mathrm{eq}}$ is a 4×4 symmetric matrix, all its eigenvalues are real numbers, and there are 4 linearly independent eigenvectors among which to choose. The unitary-norm eigenvectors are here denoted as $\hat{\boldsymbol{i}}_{\mathrm{I}}, \hat{\boldsymbol{i}}_{\mathrm{II}}, \hat{\boldsymbol{i}}_{\mathrm{III}}, \hat{\boldsymbol{i}}_{\mathrm{IV}}$, and are ordered according to their corresponding eigenvalues in a way that $\nu_{\mathrm{I}} \geq \nu_{\mathrm{II}} \geq \nu_{\mathrm{III}} \geq \nu_{\mathrm{IV}}$. In other words, $\hat{\boldsymbol{i}}_{\mathrm{I}}$ is used to denote the unitary-norm eigenvector related to the maximum (positive) eigenvalue ν_{I} of $\boldsymbol{L}'_{\mathrm{eq}}$, and $\hat{\boldsymbol{i}}_{\mathrm{IV}}$ is used to denote the unitary-norm eigenvector related to the minimum (negative) eigenvalue ν_{IV} of $\boldsymbol{L}'_{\mathrm{eq}}$. Naturally, it is worth emphasizing that, since $\boldsymbol{L}'_{\mathrm{eq}}$ is a periodic function of θ_{el}, its eigenvalues and eigenvectors are also periodic functions of θ_{el}.

Then, the optimization has been simplified from choosing among any current set to only choosing among the eigenvectors of $\boldsymbol{L}'_{\mathrm{eq}}$. The current references set can be therefore expressed as $\boldsymbol{i}^*_{\mathrm{eq}} = I^*_m \cdot \hat{\boldsymbol{i}}_k$, for $k = \mathrm{I}, \mathrm{II}, \mathrm{III}$ or IV.

By substituting $\boldsymbol{i}^*_{\mathrm{eq}} = I^*_m \cdot \hat{\boldsymbol{i}}_k$ in the torque expression (12b) and by recalling from (19) that $\hat{\boldsymbol{i}}_k^{\mathrm{T}} \cdot \boldsymbol{L}'_{\mathrm{eq}} \cdot \hat{\boldsymbol{i}}_k = \nu_k$, it results:

$$\begin{aligned} T^*_{em} &= (\boldsymbol{i}^{*\,\mathrm{T}}_{\mathrm{eq}} \cdot \boldsymbol{L}'_{\mathrm{eq}} \cdot \boldsymbol{i}^*_{\mathrm{eq}})/2 = \\ &= (I^{*\,2}_m/2)(\hat{\boldsymbol{i}}_k^{\mathrm{T}} \cdot \boldsymbol{L}'_{\mathrm{eq}} \cdot \hat{\boldsymbol{i}}_k) = \nu_k \cdot I^{*\,2}_m/2 \end{aligned} \tag{20}$$

This expression can only be solved if ν_k has the same sign of T^*_{em}, which further restricts the choice of $\hat{\boldsymbol{i}}_k$. In such case, (20) can be inverted resulting in:

$$I^*_m = \sqrt{2 \cdot T^*_{em}/\nu_k} \tag{21}$$

From (21) it can be concluded that the eigenvalue ν_k must have the same sign of T^*_{em} and that, to minimize I^*_m:

- if $T^*_{em} \geq 0$, it is convenient to select the eigenvector $\hat{\boldsymbol{i}}_{\mathrm{I}}$, related to the most positive eigenvalue $\nu_{\mathrm{I}} > 0$,
- if $T^*_{em} < 0$, it is convenient to select the eigenvector $\hat{\boldsymbol{i}}_{\mathrm{IV}}$, related to the most negative eigenvalue $\nu_{\mathrm{IV}} < 0$,

To sum up, the reference vector $\boldsymbol{i}^*_{\mathrm{eq}}$ which solves the MTPA problem (16) can be computed as:

$$\boldsymbol{i}^*_{\mathrm{eq}} = \begin{cases} \sqrt{2 \cdot T^*_{em}/\nu_{\mathrm{I}}} \cdot \hat{\boldsymbol{i}}_{\mathrm{I}} & \text{if } T^*_{em} \geq 0 \\ \sqrt{2 \cdot T^*_{em}/\nu_{\mathrm{IV}}} \cdot \hat{\boldsymbol{i}}_{\mathrm{IV}} & \text{if } T^*_{em} < 0 \end{cases} \tag{22}$$

and, as previously mentioned, the corresponding optimal phase currents $\boldsymbol{i}^*_{\mathrm{ph}}$ can be simply found by applying the inverse transformation (9) (with $i^*_0 = 0$).

C. MTPA Solution Properties and Implementation

Several interesting properties can be found from inspection of the optimal solution (22).

First, since the torque expression in (12) is a quadratic form of the currents set, once $\boldsymbol{i}^*_{eq}$ has been computed, the set $-\boldsymbol{i}^*_{eq}$ is also an optimal solution of the same MTPA problem (16). This requires some attention to guarantee a smooth behaviour of $\hat{\boldsymbol{i}}_{\mathrm{I}}$ and $\hat{\boldsymbol{i}}_{\mathrm{IV}}$ for different values of θ_{el}. In other words, considering two positions $\theta_{el,1}$ and $\theta_{el,2}$, to avoid sharp transitions in the reference currents set, it must be guaranteed that

$$\hat{\boldsymbol{i}}_{\mathrm{I}}(\theta_{el,1}) \cdot \hat{\boldsymbol{i}}_{\mathrm{I}}(\theta_{el,2}) \geq 0 \tag{23a}$$

$$\hat{\boldsymbol{i}}_{\mathrm{IV}}(\theta_{el,1}) \cdot \hat{\boldsymbol{i}}_{\mathrm{IV}}(\theta_{el,2}) \geq 0 \tag{23b}$$

This can be easily fulfilled by changing $\hat{\boldsymbol{i}}_{\mathrm{I}}(\theta_{el,2}) \rightarrow -\hat{\boldsymbol{i}}_{\mathrm{I}}(\theta_{el,2})$ or $\hat{\boldsymbol{i}}_{\mathrm{IV}}(\theta_{el,2}) \rightarrow -\hat{\boldsymbol{i}}_{\mathrm{IV}}(\theta_{el,2})$ in case one of the inequalities in (23) is not satisfied.

Additionally, the current I^*_m of the optimal solution, which is expressed by (21), is proportional to the square root of the reference torque T^*_{em}, while the overall stator losses p_{Cu}, which depend on I^2_m, are proportional to T^*_{em}. However, this proportionality depends on the value of ν_{I} or ν_{IV}. These eigenvalues may not be constant with respect to θ_{el}, meaning that the development of the same electromagnetic torque for different rotor positions may require different current magnitudes. This can be explained by considering that, in a general configuration, the variable reluctance torque may not have the same effectiveness according to the rotor position.

Moreover, in general, it may also result $\nu_{\mathrm{I}} \neq -\nu_{\mathrm{IV}}$: this would mean that (according to the position θ_{el}) the RMS current needed to develop a positive torque T^*_{em} may be different from the current needed to develop a negative torque $-T^*_{em}$. In other words, due to unequal reluctance effects, the machine may show (locally) a preferred spinning direction.

Since both the eigenvalues and the eigenvectors appearing in (22) are periodic functions of θ_{el}, the optimal currents sets $\boldsymbol{i}^*_{\mathrm{eq}}$ and $\boldsymbol{i}^*_{\mathrm{ph}}$ are also periodic with respect to θ_{el}. In general, the optimal currents may show multiple harmonics even for the generation of a constant electromagnetic torque.

For practical implementation, to reduce the required computational effort, the proposed algorithm can be executed offline for different rotor positions and for a reference torque $T^*_{em} = \pm 1\,\mathrm{N\,m}$. Then, the optimal currents, computed as per (22), can be stored in memory (e.g., through the harmonics of their Fourier decomposition) and, once applied in a real-time application, they only need to be multiplied by $\sqrt{|T^*_{em}|}$.

Finally, it is worth saying that the same approach can also be applied with no changes to machines with a different number of phases. However, this method requires a precise knowledge of the inductances, which should be properly estimated from a set of preliminary measurements. Moreover, it does not consider voltage or current limits and, therefore, it is only suited for operation in the base speed region of the machine. Note also that, for high loads, SynRMs can show a non-linear flux linkage behaviour. In that case, the algorithm would still perform to some extent, but may not be optimal. In general, the proposed approach could be properly modified to explicitly tackle the non-linearity and/or other losses, by adding more terms and/or constraints into (16). However, in that case, the problem may become extremely complicated, and a general analytical solution may not exist anymore. These variants and extensions will be analysed in future works.

IV. Algorithm Validation

The proposed algorithm has been validated with respect to the experimental setup depicted in Fig. 2.

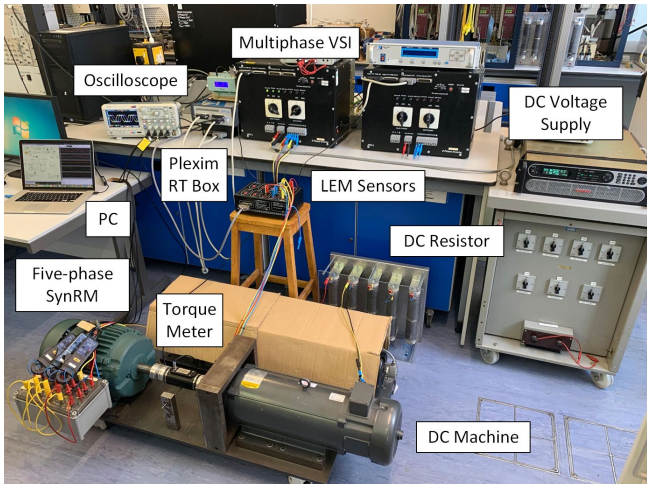

Fig. 2. Experimental Setup.

A. Analysed Machine

The considered five-phase SynRM has two pole pairs. The stator has 40 slots and the windings have a distributed layout and a symmetrical disposition in a way that the magnetic axes are mutually shifted by 72° electrically between one another. The variable reluctance rotor has been obtained by cutting an original squirrel-cage rotor of an induction machine to realize 4 salient poles as in Fig. 3. Table I summarizes the main geometrical parameters. The mechanical position θ is referred to the magnetic axis of phase 1. The DC winding resistance is the same for all the 5 phases and equal to $R = 1.8\,\Omega$.

The inductances parameters have been found in the phase variables domain. The phase 1 of the machine has been supplied with a sinusoidal voltage with a peak value of 20 V and a frequency of 50 Hz, while all the other phases have been left open. The current in phase 1 and the induced voltages in all the other phase windings $\{2, 3, 4, 5\}$ have been measured with

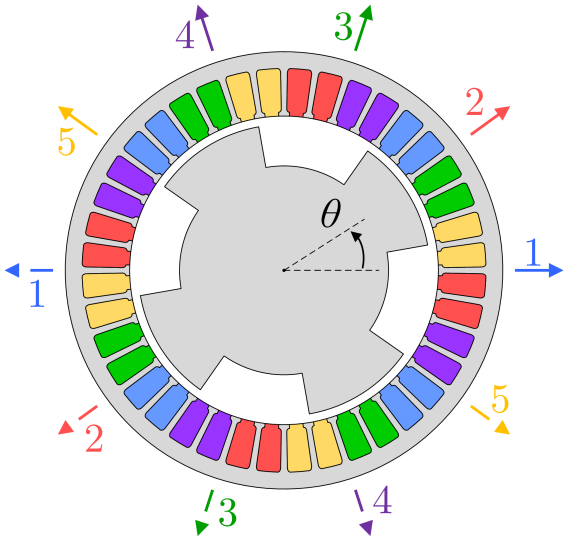

Fig. 3. Geometric representation of the five-phase synchronous reluctance machine under analysis.

TABLE I
MACHINE GEOMETRICAL DATA

Pole Pairs	2	
Internal stator diameter	127	mm
External stator diameter	180	mm
Stator slot depth	20	mm
Number of wires per slot	54	
Number of turns per phase	216	
Minimum rotor diameter	86	mm
Maximum rotor diameter	126	mm
Salient poles height	20	mm
Minimum air-gap width	0.5	mm
Maximum air-gap width	20.5	mm
Axial length	101.6	mm

the rotor locked at different positions. From the voltage and current measurements, it is possible to estimate the induced fluxes as:

$$\lambda_1(t) = \int \left(v_1(t) - R \cdot i_1(t)\right) \mathrm{d}t \tag{24a}$$

$$\lambda_k(t) = \int v_k(t)\,\mathrm{d}t, \quad (\text{with } k = 2, 3, 4, 5) \tag{24b}$$

All the fluxes have been plotted with respect to the machine current $i_1(t)$ in a way to obtain different hysteresis loops for each rotor position under test. The results are depicted in Fig. 4 for different values of $\theta_{el} = 2 \cdot \theta$. Then, to line up with the linearity approximation assumed in Section II, the parameters $L_{k,1}(\theta_{el})$ (with $k = 1, \ldots, 5$) of the first row of the inductances matrix $L_{ph}(\theta_{el})$ defined in (2) have been found with a linear regression procedure as the slope of the linear characteristics λ/i which better approximates the different hysteresis loops.

Finally, the values of $L_{k,1}(\theta_{el})$ have been extrapolated with an additional regression procedure based on the computation of the lowest even-order harmonics in θ_{el}. To be more specific, the inductances have been approximated as the superposition of a continuous component and of the harmonics varying with $2 \cdot \theta_{el}$, $6 \cdot \theta_{el}$, $10 \cdot \theta_{el}$ and $14 \cdot \theta_{el}$, and the computation of these harmonic components has been carried out while explicitly considering the symmetry properties of the machine. The results of this parameter identification procedure are reported

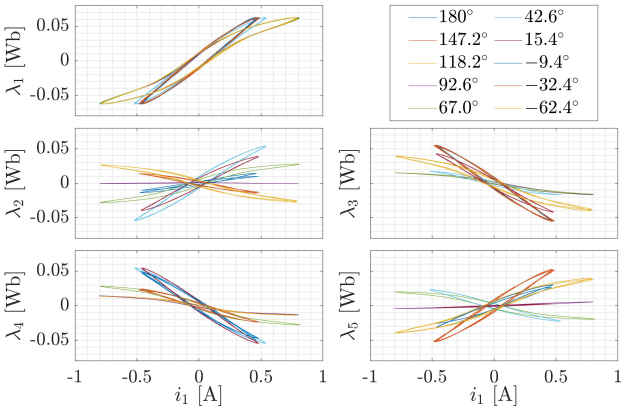

Fig. 4. Hysteresis loops obtained for different rotor positions by supplying the phase 1 with all the other phases left in open circuit.

in Table II for the inductances terms $L_{1,1}(\theta_{el})$, $L_{2,1}(\theta_{el})$ and $L_{3,1}(\theta_{el})$. Note that, because of the rotor symmetry, $L_{4,1}(\theta_{el}) = L_{3,1}(-\theta_{el})$ and $L_{5,1}(\theta_{el}) = L_{2,1}(-\theta_{el})$.

The corresponding waveforms for varying θ_{el} are shown in Fig. 5. The top graph shows the inductances functions (solid lines) and the slopes of the measured hysteresis loops of Fig. 4 (* markers) in the range $[-180°; 180°]$ of the electrical angle $\theta_{el} = 2 \cdot \theta$. The bottom graph shows the corresponding terms of the matrix $\boldsymbol{L}'_{\rm ph}(\theta_{el}) = \partial \boldsymbol{L}_{\rm ph}/\partial\theta$, which is responsible for the torque development.

As can be noted, the self-inductance $L_{1,1}(\theta_{el})$ is always positive. Its maximum value is obtained for $\theta_{el} = 0°$ and $\theta_{el} = \pm 180°$ (which is the position of minimum reluctance), while its minimum value is obtained for $\theta_{el} = \pm 90°$ (which is the position of maximum reluctance). The functions $L_{3,1}(\theta_{el})$ and $L_{4,1}(\theta_{el})$ have a mirrored symmetry with respect to θ_{el} and are always negative (coherently with the negative slopes of the corresponding hysteresis loops in Fig. 4). The functions $L_{2,1}(\theta_{el})$ and $L_{5,1}(\theta_{el})$ also have a mirrored symmetry with respect to θ_{el}, but both show positive values and negative values (coherently with the slope change in the corresponding hysteresis loops of Fig. 4). Given the machine symmetry, all the other inductances parameters $L_{h,k}(\theta_{el})$ (with $h = 2, 3, 4, 5$) of the matrix $\boldsymbol{L}_{\rm ph}(\theta_{el})$ are obtained by just shifting the functions $L_{1,k}(\theta_{el})$ by 72°. The same is also true for the matrix $\boldsymbol{L}'_{\rm ph}(\theta_{el})$.

B. Numerical Optimization Results

The MTPA algorithm developed in Section III has been numerically applied with respect to the machine parameters described in the previous sub-section.

The implementation has been developed by computing the optimal currents set $\boldsymbol{i}^*_{\rm eq} = [i^*_\alpha, i^*_\beta, i^*_x, i^*_y]^{\rm T}$ via (22) in the whole range $[-180°; 180°]$ of the electrical angle position θ_{el}. The corresponding optimal phase currents set $\boldsymbol{i}^*_{\rm ph} = [i^*_1, i^*_2, i^*_3, i^*_4, i^*_5]^{\rm T}$ is then simply computed by the inverse VSD transformation (9). The results obtained when $T^*_{em} > 0$ are depicted in Fig. 6. The top graph shows the current waveforms in the VSD domain, the middle graph shows the results in the phase variable domain, and the bottom graph shows the equivalent current I^*_m defined in (14) and resulting from (21). Since, as previously discussed, the optimal currents are proportional to $\sqrt{|T^*_{em}|}$, they have been normalized by it. The optimal currents obtained for $T^*_{em} < 0$ can also be found by applying (22). Given the machine symmetry, it can be verified that they have the same waveform as in Fig. 6 and are only shifted by 90°.

TABLE II
EXTRAPOLATED INDUCTANCES HARMONICS

Inductance Function	Harmonic Order 0	2	6	10	14
$L_{1,1}(\theta_{el})$	111 mH -	30.9 mH 0°	6.9 mH 180°	1.8 mH 0°	0.3 mH 180°
$L_{2,1}(\theta_{el})$	24.9 mH -	71.5 mH −72°	6.6 mH 144°	1.5 mH 0°	0.4 mH −144°
$L_{3,1}(\theta_{el})$	−68.6 mH -	55.5 mH −144°	6 mH 108°	0.7 mH 180°	0.3 mH 72°

In the VSD domain, it can be noted that the current i_α differs from the current i_β, and the current i_x differs from the current i_y. However, given the machine symmetry, the optimal currents in the phase variable domain have the same waveform and are just shifted from one another by 72°.

As can be seen, both in the VSD and in the phase variable domain, the desired reference currents are periodic but not sinusoidal, and clearly show a non-negligible contribution of higher-order harmonic components. For example, from the Fourier analysis of the phase variable currents, it could be verified that the odd-order harmonics up to the 13th have a non-

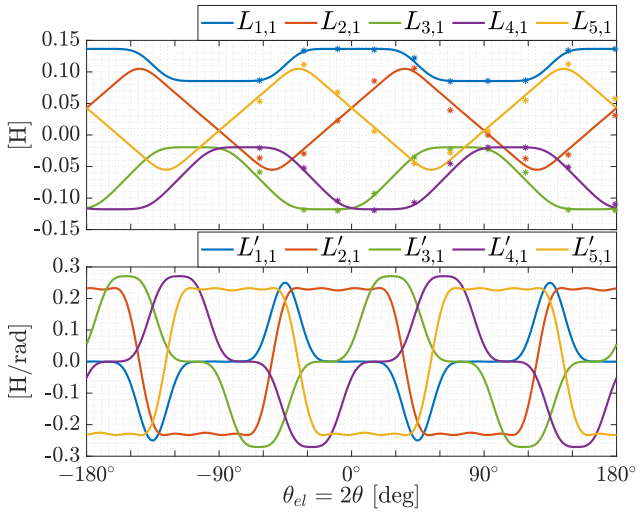

Fig. 5. Parameters of $\boldsymbol{L}_{\rm ph}(\theta_{el})$ and of $\boldsymbol{L}'_{\rm ph}(\theta_{el})$ of the examined SynRM.

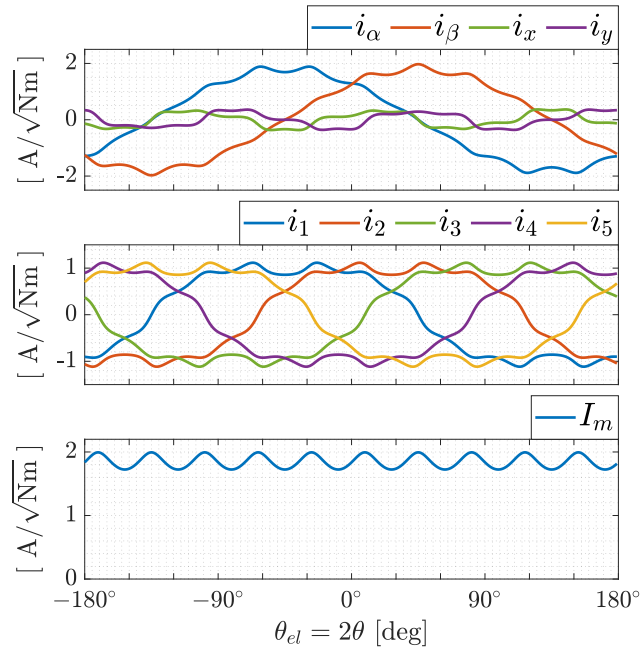

Fig. 6. Numerical optimization results in case of a positive reference torque (Top: VSD currents; Middle: Phase currents; Bottom: Equivalent overall machine current). For a negative reference torque, the optimal results have the same waveforms but shifted by 90°.

negligible contribution with respect to the fundamental (i.e., higher than 3%). However, since a constant electromagnetic torque has been imposed as a constraint in the optimization problem (16), these harmonics would not lead to any torque ripple. In other words, assuming the modelling hypothesis of Section II to be valid, the current harmonics would interact with one another in a way to produce a constant torque in the whole range of θ_{el}. Naturally, in a real prototype, there may be a torque ripple because of the non-ideal behaviour of the drive (e.g., non-ideal tracking of the optimal currents, poor knowledge of the inductances parameters, non-linear behaviour of the magnetic materials, etc…). The impact of such effects depends on the specific machine and should be analysed from case to case.

As previously mentioned, the equivalent current I_m defined in (14) identifies the magnitude of the vector $\boldsymbol{i}_{\mathrm{ph}}$ (and, from (15), also of the vectors $\boldsymbol{i}_{\mathrm{VSD}}$ and $\boldsymbol{i}_{\mathrm{eq}}$) and it can be directly associated to the overall machine stator losses. As can be seen from the bottom graph of Fig. 6, for the considered machine this current is not constant, but oscillates with a $10{\cdot}\theta_{el}$ periodicity. This means that, according to the rotor position, the development of the same electromagnetic torque may require smaller or higher currents. As an example, to develop a torque of $1\,\mathrm{N\,m}$, when $\theta_{el} = 0°$, $I_m \approx 1.8\,\mathrm{A}$, when $\theta_{el} = 9°$, $I_m \approx 2.0\,\mathrm{A}$ and when $\theta_{el} = -9°$, $I_m \approx 1.7\,\mathrm{A}$. Similarly, according to the rotor position, it could be also verified that the development of a positive torque may require a different equivalent current than the development of a negative torque. As previously mentioned, this indicates a preferred spinning direction. For example, when $\theta_{el} = 9°$, the development of $T^*_{em} = 1\,\mathrm{N\,m}$ requires an equivalent current $I_m \approx 2.0\,\mathrm{A}$ (the maximum value), while the development of $T^*_{em} = -1\,\mathrm{N\,m}$ requires $I_m \approx 1.7\,\mathrm{A}$ (the minimum value). However, this disparity effect is averaged out in a full rotor cycle, resulting in the same average value of I_m.

C. Experimental Results

The proposed strategy has been experimentally validated with the setup depicted in Fig. 2. The five-phase SynRM has been supplied through a custom-made multiphase inverter, based on Infineon FS50R12KE3 IGBT modules. The DC-bus voltage has been supplied by a Sorensen SGI600/25 single quadrant dc-voltage source and has been set to $600\,\mathrm{V}$. The multiphase SynRM is coupled to a DC machine, which has been used for mechanical loading by connecting the armature terminals to an external resistor. A Datum Electronics Torque meter M425 S1 has been positioned at the joint of the two machines to measure the torque applied at the shaft.

The control has been implemented with a Plexim RT Box 1 platform, working at $10\,\mathrm{kHz}$. The machine currents have been measured with LEM sensors, and the machine position and angular speed have been provided by a resolver. The block diagram of the control algorithm is shown in Fig. 7.

The machine speed has been regulated with a standard PI controller, that compares the error between the reference speed ω^* and the measured speed ω, and computes the reference electromagnetic torque T^*_{em} to be developed. The machine currents have been controlled in the VSD domain with a field-oriented approach. Given the presence of multiple harmonics in both the reference currents and in the induced back-EMFs, the controller has been realized with PI actions implemented in multiple synchronous reference frames, chosen according to the harmonic mapping of a five-phase machine [4]. To be more specific, the $\alpha - \beta$ current components have been regulated with PI controllers in rotating frames synchronous with θ_{el}, $-9 \cdot \theta_{el}$, $11 \cdot \theta_{el}$ and $-19 \cdot \theta_{el}$, while the $x - y$ components have been regulated with PI controllers in rotating frames synchronous with $3 \cdot \theta_{el}$, $-7 \cdot \theta_{el}$, $13 \cdot \theta_{el}$ and $-17 \cdot \theta_{el}$. The rotational matrices shown in the block diagram of Fig. 7 take the standard form:

$$\boldsymbol{D}(\vartheta) = \begin{bmatrix} \cos(\vartheta) & \sin(\vartheta) \\ -\sin(\vartheta) & \cos(\vartheta) \end{bmatrix} \tag{25}$$

with the proper choice of the rotational angle ϑ.

The computed voltage references $\boldsymbol{u}^*_{\mathrm{ph}} = \boldsymbol{C}^{\mathrm{T}} \cdot \boldsymbol{u}^*_{\mathrm{VSD}}$ are finally applied by using a PWM method. As in standard multiphase drives, a zero-sequence voltage injection (e.g., min-max injection) can be used to improve the DC-bus utilization without affecting the obtained currents [4].

To emphasize the effectiveness of the proposed MTPA strategy, it has been compared with the sole use of the fundamental current components and with the third harmonic injection strategy adopted in [15], [16].

The tests have been carried out by considering the steady-state results obtained at a constant rotor speed with a fixed loading torque. The results obtained at the speed of $750\,\mathrm{rpm}$ are depicted in Fig. 8. The figures show the VSD current components, the machine phase currents, the overall machine RMS current and the machine angular speed. The solid traces refer to the measured quantities, while the black dashed traces are the corresponding references. Fig. 9 shows the corresponding oscilloscope captures of the currents i_1 (dark blue traces), i_2 (light blue traces), and i_3 (magenta traces), and the electromagnetic torque measured at the rotor shaft (green traces, with a ratio of around $1.667\,\mathrm{Nm/V}$).

The difference between the three methods in the current waveforms can be immediately noted, both in the VSD and in the phase variables domain. When only the fundamental harmonic is exploited, the currents i_α and i_β are sinusoidal in time, while the currents i_x and i_y are zero. The third harmonic injection strategy also imposes sinusoidal i_x and i_y components, while at the same time still keeping sinusoidal i_α and i_β currents. The proposed MTPA strategy results in the non-sinusoidal current waveforms depicted in Fig. 6. It can be also seen that, for the fundamental and the third harmonic injection strategy, the current I_m (defined in (14)) is almost constant, while it instead shows a visible oscillation at around $10 \cdot \omega_{el}$ with the proposed MTPA strategy, coherently with the waveform of Fig. 6. Due to the non-idealities of the experimental setup, there are some instants in time when I_m of the proposed MTPA strategy is not the smallest one. However, it can be seen that its average value (which is related to the average RMS currents and losses) is always better than in the other methods.

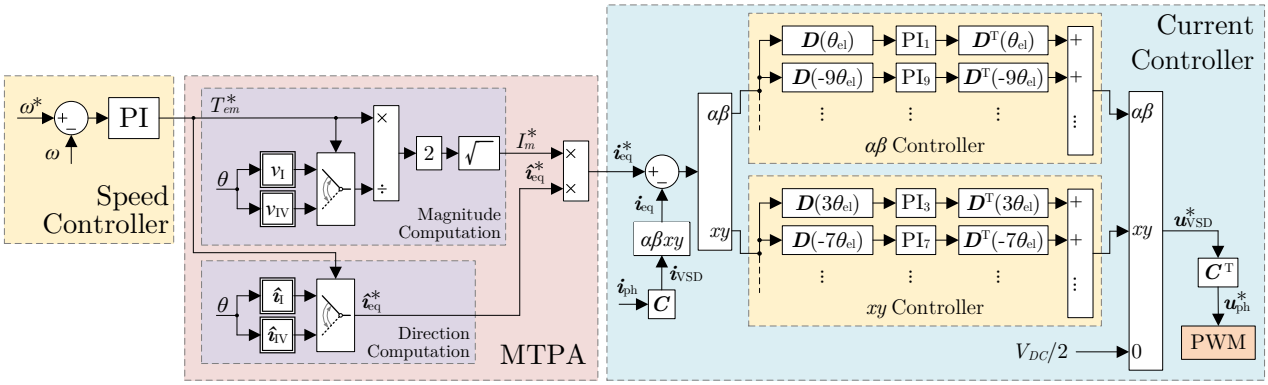

Fig. 7. Schematic block diagram of the five-phase SynRM control algorithm. The eigenvalues ν_{I},ν_{IV} and eigenvectors $\hat{\boldsymbol{\imath}}_{\mathrm{I}}$, $\hat{\boldsymbol{\imath}}_{\mathrm{IV}}$ (denoted by double-line squared blocks) are estimated based on the coefficients of their Fourier decomposition, that have been computed offline and stored in memory.

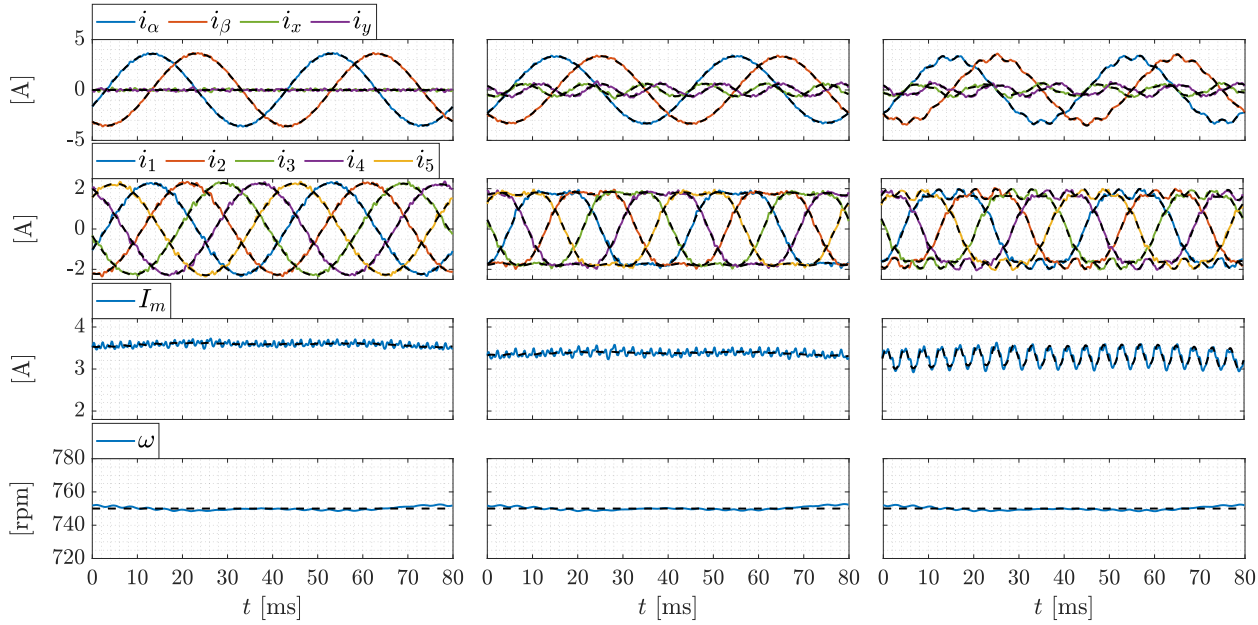

Fig. 8. Experimental results at the speed of $750\,\mathrm{rpm}$ (Left: Fundamental; Center: Third Harmonic Injection; Right: Proposed MTPA).

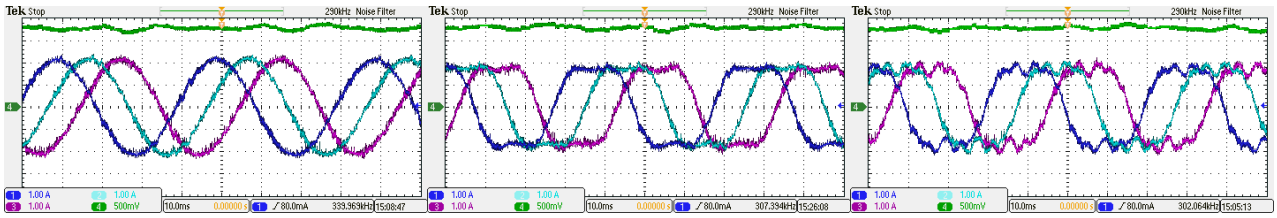

Fig. 9. Oscilloscope captures at the speed of $750\,\mathrm{rpm}$ (Left: Fundamental; Center: Third Harmonic Injection; Right: Proposed MTPA).

No sensible difference between the three methods can be instead appreciated in the measured torque and speed. This indicates that the electromagnetic torque ripple which, as previously mentioned, is inevitably due to unmodelled phenomena (e.g., the iron hysteresis behaviour or mechanical coupling effects), is not altered by the different strategies.

The same tests have also been carried out at the speeds of $375\,\mathrm{rpm}$, $500\,\mathrm{rpm}$ and $1000\,\mathrm{rpm}$. A comparison of the average Root Mean Square (RMS) current per phase obtained in a fundamental period is reported in Table III. As can be noted, in all the examined conditions the proposed MTPA strategy leads to the smallest average RMS currents, while the sinusoidal strategy is characterized by the highest values. Table IV shows the reduction of the RMS currents and of the overall stator losses obtained by the third harmonic injection strategy and by the proposed MTPA approach (when compared

TABLE III
COMPARISON OF THE AVERAGE RMS CURRENT PER PHASE

Mechanical Speed	Sinusoidal Currents Strategy	Third Harmonic Injection Strategy	Proposed MTPA
375 rpm	1.147 A	1.115 A	1.104 A
500 rpm	1.303 A	1.254 A	1.242 A
750 rpm	1.537 A	1.490 A	1.472 A
1000 rpm	1.787 A	1.714 A	1.693 A

TABLE IV
RMS CURRENT AND STATOR LOSSES REDUCTION

Mechanical Speed	Third Harmonic Injection		Proposed MTPA	
	I_{RMS}	p_{Cu}	I_{RMS}	p_{Cu}
375 rpm	−2.79%	−5.50%	−3.75%	−7.36%
500 rpm	−3.75%	−7.38%	−4.68%	−9.14%
750 rpm	−3.06%	−6.02%	−4.23%	−8.28%
1000 rpm	−4.09%	−8.00%	−5.26%	−10.24%

to the sinusoidal currents strategy) in all the considered tests.

Finally, Fig. 10 shows the performance of the proposed MTPA approach during a speed transient from $-500\,\mathrm{rpm}$ to $500\,\mathrm{rpm}$ (thus including a speed inversion), while Fig. 11 shows the response after a step change of the loading torque at $750\,\mathrm{rpm}$ (from around $3\,\mathrm{N\,m}$ to around $6\,\mathrm{N\,m}$). Both results show the machine currents (in both the VSD and phase variable domain), the developed electromagnetic torque and the rotor speed (solid traces represent measured and dashed traces reference values). As can be noted, the drive shows a satisfactory dynamic behaviour, and the currents properly follow the corresponding references even during the transients. The results also show the aforementioned 90° shift between the currents when $T^*_{em} < 0$ (during the initial time interval in Fig. 10) and when $T^*_{em} > 0$ (after the speed inversion).

V. CONCLUSIONS

This paper proposed an MTPA algorithm for a five-phase synchronous reluctance machine drive. The algorithm has been addressed considering generalized machine parameters, and has been formalized as a constrained optimization problem, aimed at the minimization of an overall equivalent machine current for a given reference electromagnetic torque to be developed. The optimal solution has been computed analytically in the VSD domain, and it depends on the eigenvectors of the inductance derivatives matrix. The algorithm has been validated both numerically and experimentally with respect to a specific five-phase salient-pole SynRM prototype. Considering the inductances of the machine, the optimal currents are highly non-sinusoidal, and have been controlled with PI controllers in multiple rotating reference frames. The proposed approach has also been compared with other current references computation strategies, being the use of sinusoidal currents and the third harmonic injection strategy. The results show that the proposed MTPA solution is characterized by smaller RMS currents (and overall stator losses) with respect to the other approaches applied in the same operating conditions. The same approach can be applied, with relatively low modifications, also for a different number of phases. Some extensions for future investigations include the explicit consideration of the machine non-linearities and the adaption of the proposed technique to different requirements and/or operating conditions (e.g., overall losses minimization, voltage/current limits and flux weakening operations).

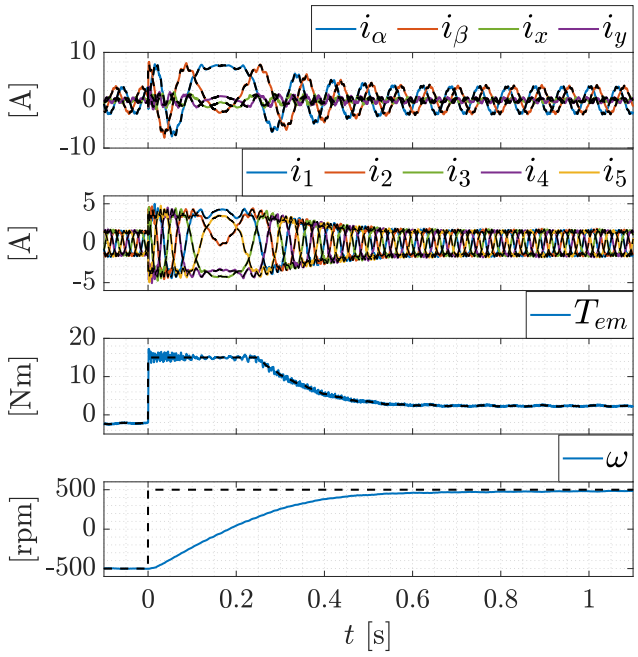

Fig. 10. Experimental results in the speed inversion test.

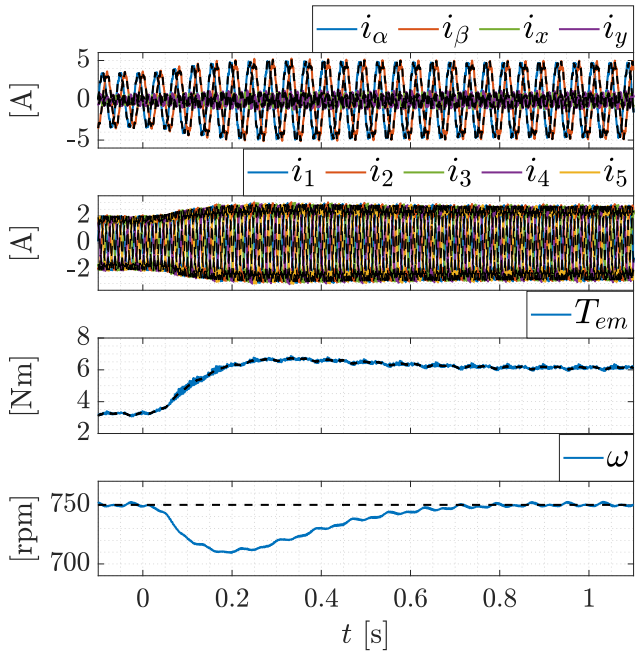

Fig. 11. Experimental results with a step change of the loading torque.

REFERENCES

[1] A. Fratta and A. Vagati, "A reluctance motor drive for high dynamic performance application," *IEEE Trans. Ind. Appl.*, vol. 28, DOI 10.1109/28.148454, no. 4, pp. 873–879, 1992.

[2] T. Matsuo and T. Lipo, "Field oriented control of synchronous reluctance machine," in *Proceedings of IEEE Power Electronics Specialist Conference - PESC '93*, DOI 10.1109/PESC.1993.471965, pp. 425–431, 1993.

[3] J. Kolehmainen, "Synchronous reluctance motor with form blocked rotor," *IEEE Trans. Energy Convers.*, vol. 25, DOI 10.1109/TEC.2009.2038579, no. 2, pp. 450–456, 2010.

[4] E. Levi, "Multiphase electric machines for variable-speed applications," *IEEE Trans. Ind. Electron.*, vol. 55, DOI 10.1109/TIE.2008.918488, no. 5, pp. 1893–1909, 2008.

[5] F. Barrero and M. J. Duran, "Recent advances in the design, modeling, and control of multiphase machines-part i," *IEEE Trans. Ind. Electron.*, vol. 63, DOI 10.1109/TIE.2015.2447733, no. 1, pp. 449–458, 2016.

[6] M. J. Duran and F. Barrero, "Recent advances in the design, modeling, and control of multiphase machines-part ii," *IEEE Trans. Ind. Electron.*, vol. 63, DOI 10.1109/TIE.2015.2448211, no. 1, pp. 459–468, 2016.

[7] R. Betz, R. Lagerquist, M. Jovanovic, T. Miller, and R. Middleton, "Control of synchronous reluctance machines," *IEEE Trans. Ind. Appl.*, vol. 29, DOI 10.1109/28.259721, no. 6, pp. 1110–1122, 1993.

[8] E. Rashad, T. Radwan, and M. Rahman, "A maximum torque per ampere vector control strategy for synchronous reluctance motors considering saturation and iron losses," in *Conference Record of the 2004 IEEE Industry Applications Conference, 2004. 39th IAS Annual Meeting.*, vol. 4, DOI 10.1109/IAS.2004.1348813, pp. 2411–2417 vol.4, 2004.

[9] T. Senjyu, K. Kinjo, N. Urasaki, and K. Uezato, "High efficiency control of synchronous reluctance motors using extended kalman filter," *IEEE Trans. Ind. Electron.*, vol. 50, DOI 10.1109/TIE.2003.814998, no. 4, pp. 726–732, 2003.

[10] P. Niazi, H. A. Toliyat, and A. Goodarzi, "Robust maximum torque per ampere (mtpa) control of pm-assisted synrm for traction applications," *IEEE Trans. Veh. Technol.*, vol. 56, DOI 10.1109/TVT.2007.896974, no. 4, pp. 1538–1545, 2007.

[11] J. Ahn, S. Lim, K.-C. Kim, J. Lee, J.-H. Choi, S. Kim, and J.-P. Hong, "Field weakening control of synchronous reluctance motor for electric power steering," *IET Electric Power Applications*, vol. 1, pp. 565–570, Jul. 2007.

[12] G. H. B. Foo and X. Zhang, "Robust direct torque control of synchronous reluctance motor drives in the field-weakening region," *IEEE Trans. Power Electron.*, vol. 32, DOI 10.1109/TPEL.2016.2542241, no. 2, pp. 1289–1298, 2017.

[13] H. Eldeeb, C. M. Hackl, L. Horlbeck, and J. Kullick, "A unified theory for optimal feedforward torque control of anisotropic synchronous machines," *International Journal of Control*, vol. 91, DOI 10.1080/00207179.2017.1338359, no. 10, pp. 2273–2302, 2018.

[14] A. Accetta, M. Cirrincione, M. C. D. Piazza, G. L. Tona, M. Luna, and M. Pucci, "Analytical formulation of a maximum torque per ampere (mtpa) technique for synrms considering the magnetic saturation," *IEEE Trans. Ind. Appl.*, vol. 56, DOI 10.1109/TIA.2020.2993525, no. 4, pp. 3846–3854, 2020.

[15] H. Toliyat, L. Xu, and T. Lipo, "A five-phase reluctance motor with high specific torque," *IEEE Trans. Ind. Appl.*, vol. 28, DOI 10.1109/28.137454, no. 3, pp. 659–667, 1992.

[16] H. Toliyat, S. Waikar, and T. Lipo, "Analysis and simulation of five-phase synchronous reluctance machines including third harmonic of airgap mmf," *IEEE Trans. Ind. Appl.*, vol. 34, DOI 10.1109/28.663476, no. 2, pp. 332–339, 1998.

[17] H. Toliyat, L. Xu, and T. Lipo, "A five phase reluctance motor, with high specific torque," in *Conference Record of the 1990 IEEE Industry Applications Society Annual Meeting*, DOI 10.1109/IAS.1990.152188, pp. 207–213 vol.1, 1990.

[18] L. Xu, "Rotor structure selections of nonsine five-phase synchronous reluctance machines for improved torque capability," *IEEE Trans. Ind. Appl.*, vol. 36, DOI 10.1109/28.855967, no. 4, pp. 1111–1117, 2000.

[19] L. Xu and B. Wang, "Comparison study of rotor structures for five-phase synchronous reluctance machines," in *Conference Record of the 1999 IEEE Industry Applications Conference. Thirty-Forth IAS Annual Meeting (Cat. No.99CH36370)*, vol. 2, DOI 10.1109/IAS.1999.801608, pp. 846–853 vol.2, 1999.

[22] M. Muteba, "Influence of mixed stator winding configurations and number of rotor flux-barriers on torque and torque ripple of five-phase

[20] J. Law, A. Chertok, and T. Lipo, "Design and performance of field regulated reluctance machine," *IEEE Trans. Ind. Appl.*, vol. 30, DOI 10.1109/28.315228, no. 5, pp. 1185–1192, 1994.

[21] C. Coates, D. Platt, and V. Gosbell, "Performance evaluation of a nine-phase synchronous reluctance drive," in *Conference Record of the 2001 IEEE Industry Applications Conference. 36th IAS Annual Meeting (Cat. No.01CH37248)*, vol. 3, DOI 10.1109/IAS.2001.955908, pp. 2041–2047 vol.3, 2001.
synchronous reluctance motors," in *2019 IEEE Transportation Electrification Conference and Expo (ITEC)*, DOI 10.1109/ITEC.2019.8790614, pp. 1–6, 2019.

[23] Q. Chen, X. Shi, G. Xu, and W. Zhao, "Torque calculation of five-phase synchronous reluctance motors with shifted-asymmetrical-salient-poles under saturation condition," *CES Transactions on Electrical Machines and Systems*, vol. 4, DOI 10.30941/CESTEMS.2020.00015, no. 2, pp. 105–113, 2020.

[24] T. Kumagai, J.-i. Itoh, and K. Kusaka, "Reduction method of torque ripple, dc current ripple, and radial force ripple with control flexibility of five-phase srm," in *2020 IEEE Energy Conversion Congress and Exposition (ECCE)*, DOI 10.1109/ECCE44975.2020.9236039, pp. 4703–4708, 2020.

[25] K. B. Tawfiq, M. N. Ibrahim, E. E. EL-Kholy, and P. Sergeant, "Performance analysis of a rewound multiphase synchronous reluctance machine," *IEEE Journal of Emerging and Selected Topics in Power Electronics*, DOI 10.1109/JESTPE.2021.3106591, pp. 1–1, 2021.

[26] Z. Zhang, "A robust non-permanent magnet five-phase synchronous reluctance traction motor," in *2021 IEEE Transportation Electrification Conference Expo (ITEC)*, DOI 10.1109/ITEC51675.2021.9490116, pp. 1–6, 2021.

[27] G. Grandi, G. Serra, and A. Tani, "General analysis of multiphase systems based on space vector approach," in *2006 12th International Power Electronics and Motion Control Conference*, DOI 10.1109/EPEPEMC.2006.4778503, pp. 834–840, 2006.

[28] A. Tessarolo, "On the modeling of poly-phase electric machines through vector-space decomposition: Theoretical considerations," in *2009 International Conference on Power Engineering, Energy and Electrical Drives*, DOI 10.1109/POWERENG.2009.4915234, pp. 519–523, 2009.

Andrea Cervone (Student Member, IEEE) received the B.Sc. and M.Sc. and PhD degrees in electrical engineering in 2014, 2017 and 2021, respectively, from the University of Naples Federico II, Naples, Italy. His research interests include multilevel converters and multiphase electrical drives.

Obrad Dordevic (S'11, M'13) received his Dipl. Ing. degree in Electronic Engineering from the University of Belgrade, Serbia, in 2008. He joined Liverpool John Moores University in December 2009 as a PhD student. Dr. Dordevic received his PhD degree in April 2013 and was appointed as a Lecturer at the Liverpool John Moores University in May 2013. In 2018 he was promoted to a Reader in Power Electronics. His main research interests are in the areas of power electronics, electrostatic precipitators, and advanced variable speed multiphase drive systems.